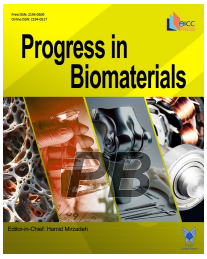

Volume 13, Issue 2, 132407 (1-8)

Progress in Biomaterials (PIBM)

https://doi.org/10.57647/pibm.2024.132407

Synthesis and Characterization of Nano-Hydroxyapatite Containing Titanium Oxide Nanoparticles for Dental Applications

Masoumeh Tabatabaee[1], Mahboubeh A. Sharif[2]*, Saeid Hassan Shahi[3], Mahbubeh Mahmoudi[3]

[1]*Department of Chemistry, Ya.C., Islamic Azad University, Yazd, Iran.*
[2]*Department of Chemistry, Qo.C., Islamic Azad University, Qom, Iran.*
[3]*Department of Biomedical Engineering, Ya.C., Islamic Azad University, Yazd, Iran.*

*__Corresponding author:__ ma.sharif@iau.ac.ir

Original Research

Abstract:

Despite significant advancements in dental composite technologies, effective treatment of oral diseases remains a clinical challenge. This study focuses on the synthesis and characterization of hydroxyapatite (HAp) powder modified with titanium oxide (TiO_2) nanoparticles, aiming to enhance its physicochemical and biological properties for dental applications. The composite was synthesized via the sol–gel method, and its structural integrity was confirmed through Fourier Transform Infrared Spectroscopy (FTIR) and X-ray Diffraction (XRD), indicating successful formation of the HAp phase. Scanning Electron Microscopy (SEM) revealed a uniform distribution of TiO_2 nanoparticles and strong interfacial bonding within the HAp matrix. Thermogravimetric Analysis (TGA) demonstrated improved thermal stability in the TiO_2-doped HAp compared to pure HAp. Biocompatibility was assessed using the MTT assay on osteoblast cells, showing 82% cell viability, which reflects excellent cytocompatibility. These results suggest that TiO_2 incorporation not only enhances the thermal and structural properties of hydroxyapatite but also supports cell proliferation, making it a promising candidate for dental restoration and broader biomedical applications. The study provides a foundation for future development of bioactive materials tailored for regenerative dentistry and implantology.

Keywords:

Hydroxyapatite (HAp); Titanium oxide nanoparticles (TiO_2); Sol–gel synthesis; Osteoblast cells; Dental materials; Biomedical applications

Cite this article: Tabatabaee, M., Sharif, M.A., Shahi, S.H., Mahmoudi, M. Synthesis and Characterization of Nano-Hydroxyapatite Containing Titanium Oxide Nanoparticles for Dental Applications. *Progress in Biomaterials* **13**(2), Article 07 (2024).

1. Introduction

Oral and dental diseases continue to represent a major global public health concern due to their high prevalence, chronic nature, and impact on quality of life. These conditions, particularly periodontal disease and dental caries, are among the most common infections affecting humans and are closely linked to systemic health outcomes such as cardiovascular disease, diabetes, and adverse pregnancy events (Murad and Fadhala, 2023; Janakiram et al., 2018; Wolf et al., 2021). Despite advances in preventive and restorative dentistry, millions of people worldwide suffer from untreated dental conditions, leading to functional impairment, pain, and aesthetic concerns. Previous reports have shown that a considerable portion of annual public healthcare expenditures is allocated to the care or treatment of damaged teeth (Hung et al., 2020; Jevdjevic et al., 2020). The economic burden of oral diseases is substantial (Alzahrani et al., 2022). According to the World Health Organization (WHO, 2022), global spending on oral healthcare exceeds US$ 400 billion annually, accounting for a significant portion of healthcare budgets in both developed and developing countries. In the United States alone, direct dental care expenditures were estimated at US$ 155 billion in 2021, reflecting the persistent cost burden of restorative and surgical procedures (American Dental Association, 2022). Periodontal disease (gum inflammation) is a common and complex inflammatory disorder characterized by the destruction of

the soft and hard supporting tissues surrounding the teeth. If left untreated, the disease can progress to involve the dental pulp. Various factors-such as dental plaque, smoking, and underlying conditions like diabetes-can significantly increase the risk of developing this disease (Silva et al., 2018). According to previous studies, this disease is one of the most common causes of tooth loss in childhood and edentulism (toothlessness) in adulthood. Furthermore, due to its infectious nature, periodontal disease can act as a risk factor for preterm birth and low birth weight in newborns. Dental caries is among the most prevalent chronic diseases affecting children and adolescents worldwide (Kaneko et al., 2018; Demarco et al., 2011). Dental caries is defined as an infectious, microbial, and transmissible disease of the tooth tissues that leads to demineralization of inorganic components and destruction of the organic matrix of the tooth. The formation of cavities (tooth surface destruction) is a clinical sign of bacterial infection. Several factors influence the onset and progression of dental caries, including oral environmental conditions, fermentable carbohydrates, cariogenic microorganisms, and the duration of exposure necessary for decay to occur. One of the major challenges in the field of dentistry is related to the materials used for treatment and restoration (Abidi and Murtaza, 2014; Roberts et al., 2022). Dental materials must possess high strength and hardness while also exhibiting an aesthetically pleasing appearance. Poor formulation of dental materials can lead to discomfort, adverse side effects, and increased healthcare costs. Bioceramic is a type of ceramic biomaterial-meaning a ceramic substance that can replace or enhance the function of tissues or organs in the human body (Ramesh et al., 2013; Blatz et al., 2019).

The main medical applications of bioceramics are in dentistry and orthopedics. Among various types of bioceramics, the calcium phosphate family holds particular importance because of its structural and chemical similarity to the hard tissues of the body (bones and teeth). Moreover, its main components-phosphate and calcium ions-are naturally present in the human body. These features make this family of bioceramics highly biocompatible (Albulescu et al., 2019; Eliaz and Metoki, 2017). Among calcium phosphates, hydroxyapatite is the most thermodynamically stable phase under physiological temperature and body conditions. The crystalline structure of hydroxyapatite closely resembles the mineral phase that constitutes human bones and teeth (Weng et al., 2000; Eliaz and Metoki, 2017; Roveri et al., 2017). Hydroxyapatite has extensive applications in medicine and dentistry, including bone tissue replacement and implant coating. It exhibits several advantageous properties, such as higher mechanical strength and better biocompatibility compared to its micrometer-sized counterparts, uniform particle size and shape with minimal agglomeration, favorable interactions with bone tissues that promote bone cell adhesion and growth, and more suitable density compared to other commonly used materials (Awasthi et al., 2020; Ma et al., 2017). The most significant characteristic of hydroxyapatite that makes it highly attractive to materials and biomaterials researchers is its biological properties. Hydroxyapatite possesses important features such as bioactivity and osteoconductivity. Bioactivity refers to the ability of a material to form a direct chemical bond with living cells, while osteoconductivity denotes the capacity to support and guide bone growth. In other words, hydroxyapatite can facilitate and stimulate the regeneration of lost bone tissue when implanted in the body (Filip et al., 2022). Currently, most bioceramics used in dental materials and dentistry are based on titanium, magnesium, and zirconium. In this study, the potential application of hydroxyapatite-based bioceramics, synthesized using nano-calcium oxide with specific ratios and high mechanical strength, is investigated to meet the practical needs of dental professionals (Jarcho et al., 1976; Hanawa, 2020). Recent advancements in biomaterials research have focused on developing cost-effective and scalable strategies for synthesizing hydroxyapatite (HAp) nanoparticles with enhanced physicochemical performance. Studies published after 2015 have introduced improved fabrication routes that not only optimize nanoparticle morphology but also significantly strengthen their mechanical integrity. For example, researchers have demonstrated that incorporating hardystonite a next-generation bioactive ceramic-into HAp formulations can markedly improve toughness and structural stability while preserving the material's high biocompatibility, making it suitable for dental and orthopedic applications (Pushpalatha et al., 2023; Balhuc et al., 2021; Anil et al., 2022; Iftikhar et al., 2021). In parallel, investigations carried out between 2016 and 2022 have provided deeper insights into ceramic-matrix nanocomposites (CMNCs) based on hydroxyapatite as a principal structural component in dental tissues. These studies confirmed that HAp reinforced with secondary ceramic phases or metallic constituents-whether processed as nano powders, lamellar structures, or fiber-reinforced composites-exhibits superior mechanical behavior and enhanced durability, thereby supporting the continued development of advanced ceramic matrix composites for dental restoration and regenerative applications (Pushpalatha et al., 2023; Balhuc et al., 2021; Seesala et al., 2023; Syed et al., 2020). More recent finite-element analyses (2017–2023) have also evaluated the influence of hydroxyapatite coating thickness on stress distribution at the implant–bone interface. Findings consistently show that optimized HAp coatings effectively reduce localized stresses within the alveolar bone, promoting greater implant stability and accelerating osseointegration. These results reaffirm that hydroxyapatite, as a bioactive and osteoconductive coating material, plays a vital role in improving long-term implant performance and clinical outcomes (Chamrad et al., 2021; Homa et al., 2024; Beig et al., 2020). Although contemporary dental bioceramics primarily rely on titanium-, magnesium-, and zirconium-based systems, emerging research trends highlight the potential of hydroxyapatite-based bioceramics engineered with nano-calcium oxide additives. These newly formulated materials, designed with controlled compositions and improved mechanical strength, are being explored as promising candidates to address the evolving clinical demands of modern dentistry (Hussein et al., 2020; Gaihre and Jayasuriya, 2018). Therefore, in this study, we aim to synthesize and characterize TiO_2-modified hydroxyapatite

using a sol–gel approach and evaluate its structural, thermal, and biological performance to determine its suitability for advanced dental applications.

2. Materials and methods

2.1 Materials

Calcium nitrate [$Ca(NO_3)_2 \cdot 4H_2O$] and titanium dioxide (TiO_2) nanoparticles were purchased from Cemfix Company (France). Tartaric acid, diammonium hydrogen phosphate, ethanol, and DMSO solution were obtained from Merck (Germany). Low-glucose DMEM, FBS, Trypsin-EDTA, and PBS were supplied by Zist Ideh Company (Iran). MTT powder was purchased from Sigma-Aldrich (USA).

2.2 Synthesis of hydroxyapatite

2.2.1 Synthesis of calcium oxide nanoparticles

First, 11.8 g of calcium nitrate (0.05 mol, 100 mol%) was weighed and mixed with 100 mL of an aqueous solution containing 7.5 mL of tartaric acid (0.10 mol, 200 mol%). The resulting solution was homogenized at room temperature for 30 minutes using a magnetic stirrer. The mixture was then subjected to hydrothermal treatment at 130 °C for 8 hours. Afterward, it was stored in a refrigerator for 2 days until the solution became concentrated and viscous. Finally, the thickened solution was calcined at 700 °C for 3 hours to obtain a white powder of calcium oxide nanoparticles.

2.2.2 Synthesis of hydroxyapatite without titanium oxide nanoparticles

Hydroxyapatite was synthesized using the sol–gel method (Guo et al., 2020). A total of 2.2 g of the prepared calcium oxide nanoparticles (0.04 mol CaO, 100 mol%) was mixed with 100 mL of water and stirred for 24 hours. Then, a 0.5 M phosphoric acid solution was prepared and added dropwise to the suspension until the pH reached 8.5-9.5. The molar ratio of CaO to H_3PO_4 was maintained at approximately 1.67, corresponding to the stoichiometry of hydroxyapatite ($Ca/P = 1.67$). The mixture was stirred for 5 hours, cooled, and then frozen for complete precipitation. The precipitate was washed and dried at 120 °C for 4 hours. This sample was considered the control.

2.2.3 Synthesis of hydroxyapatite containing titanium oxide nanoparticles

The same procedure was followed, except that 1 g of TiO_2 nanoparticles (0.012 mol, corresponding to ~ 20 mol% relative to CaO) was added to the suspension before the phosphoric acid addition. The $CaO/TiO_2/H_3PO_4$ molar ratio was adjusted to maintain $Ca/P = 1.67$ while incorporating TiO_2 as a dopant. All subsequent steps were identical to the control synthesis.

2.3 Characterization of the samples

2.3.1 Scanning electron microscopy (SEM)

Prior to SEM observation, the samples were placed in an oven at 60 °C to remove any possible moisture, and then sputter-coated with gold for 150 seconds. The samples were subsequently examined using a Zeiss Sigma SEM (Germany). Particle size was determined by averaging the measured particle dimensions obtained from the SEM images using EXCEL software (Ignjatović et al., 1999).

2.3.2 Fourier transform infrared spectroscopy (FTIR)

FTIR analysis was performed for calcium oxide nanoparticles and the synthesized hydroxyapatite powders in the wavenumber range of 400-4000 cm^{-1} using the Bruker Tensor 27 FTIR spectrometer (Germany) with the (ATR) method (Ignjatović et al., 1999). The spectra were recorded with a resolution of 4 cm^{-1}, and each sample was scanned 32 times to ensure reproducibility.

2.3.3 X-ray diffraction (XRD)

The structural properties and phase composition of the coatings were evaluated using a PANalytical X'Pert PRO diffractometer (Netherlands) with Cu Kα radiation ($\lambda = 1.791$ Å), operated at 30 kV and 20 mA, within a 2θ range of 20°-120°. Phase identification was performed using X'Pert software (Guma et al., 2012).

2.3.4 Thermogravimetric analysis (TGA)

Thermal stability was evaluated using a STA 503 BAHR thermogravimetric analyzer (Germany) with a heating rate of 10 °C/min under an argon atmosphere, up to 800 °C.

2.4 Cytotoxicity assessment

2.4.1 Cell culture

For cell culture and evaluation of cell viability on hydroxyapatite samples containing titanium oxide nanoparticles, osteoblast cell lines (MC3T3-E1, mouse pre-osteoblasts) were used. Frozen cells were thawed and transferred into a culture medium containing 10% newborn calf serum (NCS) and 200 µL of Penicillin–Streptomycin (Pen-Strep, 100 U/mL penicillin and 100 µg/mL streptomycin). The suspension was then transferred into a cell culture flask and incubated under conditions of 5% CO_2 and 98% humidity. After two passages, the cells were used for conducting the experiments on the samples (Lewallen et al., 2016; Abdalhay et al., 2014).

2.4.2 Cytotoxicity test

To evaluate cell proliferation and cytotoxicity, sterilized hydroxyapatite samples (with and without TiO_2 nanoparticles) were placed in the wells of a 12-well culture plate. Osteoblast cells (1×10^4 cells/well) suspended in 150 µL of culture medium were seeded onto each sample and incubated for 24 hours. Negative controls (cells cultured without samples) and positive controls (cells treated with 0.1% Triton X-100 to induce cytotoxicity) were included.

After incubation, the culture medium was removed and replaced with 150 µL of MTT solution (0.5 mg/mL in PBS). Plates were incubated for 4 hours at 37 °C to allow mitochondrial dehydrogenases in viable cells to reduce MTT into insoluble purple formazan crystals. The MTT solution was then discarded, and 150 µL of isopropanol was added to dissolve the crystals. To enhance dissolution, plates were placed on a shaker for 15 minutes.

Subsequently, 100 µL of the resulting solution from each well was transferred into a 96-well plate, and absorbance was measured at 570 nm using an ELISA microplate reader

(BioTek, USA). Wells containing a higher number of viable cells exhibited greater optical density (OD). Cell viability (%) and cytotoxicity (%) were calculated according to equations (1) and (2) (Chen et al., 2015):

$$\text{Toxicity}\% = \left(1 - \frac{\text{mean OD of sample}}{\text{mean OD of control}}\right) \times 100 \quad (1)$$

$$\text{Viability}\% = 100 - \text{Toxicity}\% \quad (2)$$

2.5 Statistical analysis of the results

All experiments were performed in triplicate, and results were expressed as mean ± standard deviation (SD). Statistical significance was determined using the Student's t-test, with $p < 0.05$ considered significant.

3. Results and discussion

3.1 Scanning electron microscopy (SEM) analysis

Figure 1 shows the SEM micrographs of hydroxyapatite powder containing and lacking titanium oxide nanoparticles. The images reveal that the powders exhibit agglomerated structures. This agglomeration may be attributed to heating and the surface tension of nanoparticles, which can lead to an apparent increase in particle size to the micrometer range (Ignjatović et al., 1999).

The SEM images also indicate that the synthesized hydroxyapatite particles are in the nanometer scale. The morphology shows cluster-like structures, and in some regions, rod-like particles are observed. Therefore, the synthesized hydroxyapatite can be highly suitable for composite fabrication or dental repair applications.

The average particle sizes obtained from SEM image analysis were 57.42 ± 13.26 nm for hydroxyapatite synthesized with titanium oxide nanoparticles and 51.89 ± 9.19 nm for hydroxyapatite synthesized without titanium oxide nanoparticles.

3.2 Fourier transform infrared spectroscopy (FTIR) analysis

Figure 2 shows the FTIR spectra of the synthesized hydroxyapatite powders. The broad absorption band observed around 3400 cm^{-1} corresponds to the stretching vibrations of hydroxyl (OH) groups, confirming the presence of structural hydroxyls in hydroxyapatite. The characteristic stretching and bending modes of phosphate (PO_4^{3-}) groups are clearly visible at 671-675 cm^{-1} and in the range of 980-1200 cm^{-1}, while a small absorption band at approximately 945 cm^{-1} is attributed to the P–O bond in hydroxyapatite. Additionally, the absorption band observed at 874 cm^{-1} corresponds to carbonate (C–O) vibrations, indicating minor substitution of carbonate ions within the apatite lattice.

Importantly, in the TiO_2-modified hydroxyapatite samples, additional spectral features can be identified. Titanium dioxide exhibits characteristic Ti–O stretching vibrations in the 400-800 cm^{-1} region. In these spectra, the shoulder near 670-675 cm^{-1} may represent overlapping contributions from both PO_4^{3-} bending and Ti–O stretching, suggesting successful incorporation of TiO_2 nanoparticles into the hydroxyapatite matrix. Furthermore, the band near 945 cm^{-1}, while primarily associated with P–O stretching, may also reflect Ti–O–P interactions, indicating chemical bonding or surface complexation between TiO_2 and phosphate groups. The incorporation of TiO_2 also influences the vibrational behavior of OH and PO_4^{3-} groups. A slight shift and reduction in intensity of the OH stretching band ($\sim$ 3400 cm^{-1}) was observed, which can be attributed to hydrogen bonding or partial substitution effects caused by TiO_2 nanoparticles. Similarly, subtle changes in the PO_4^{3-} stretching region (980-1200 cm^{-1}) indicate lattice distortion and enhanced crystallinity, consistent with the XRD results. These modifications confirm that TiO_2 nanoparticles are not only physically dispersed but also chemically interacting with the hydroxyapatite framework, thereby improving structural sta-

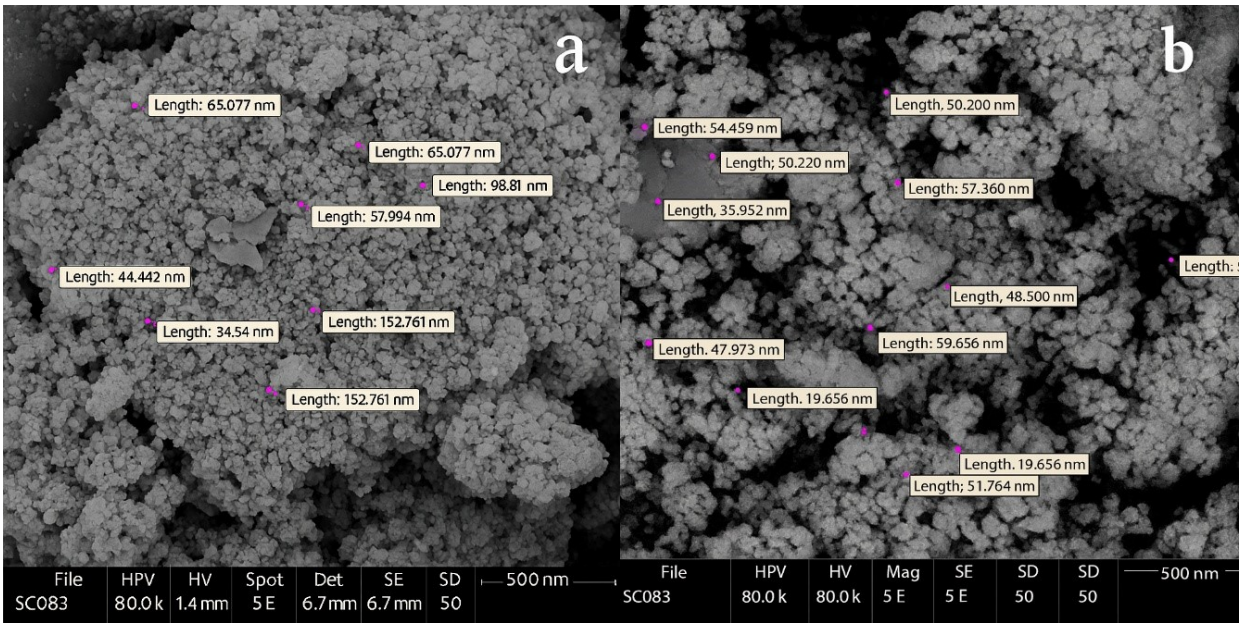

Figure 1. SEM images of hydroxyapatite powders: (a) hydroxyapatite containing titanium oxide nanoparticles, (b) hydroxyapatite without titanium oxide nanoparticles.

bility and interfacial bonding (Praveen et al., 2014; Soysal et al., 2011).

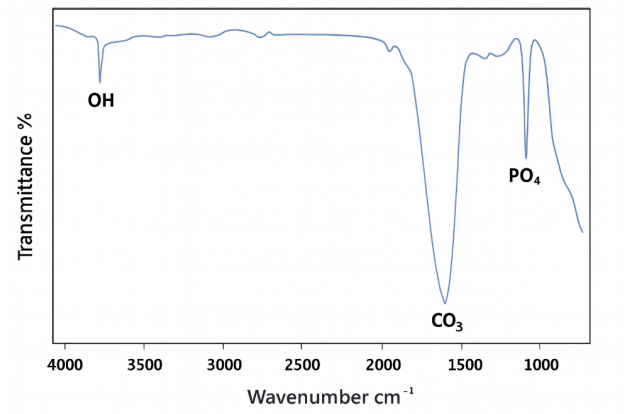

Figure 2. FTIR spectrum of the synthesized hydroxyapatite powder.

3.3 X-ray diffraction (XRD) pattern analysis

Figure 3 presents the XRD patterns of hydroxyapatite powders synthesized in the presence and absence of titanium oxide. As shown in the figure, hydroxyapatite is the only phase formed. The characteristic peaks of hydroxyapatite appear in the 2θ range of 25-35°. Similar results and peak positions have been reported in the study by Scherer et al., although their hydroxyapatite synthesis method was mechanical rather than chemical (Guma et al., 2012). As illustrated in Fig. 3 a), the characteristic hydroxyapatite peaks in the powders synthesized with titanium oxide exhibit higher intensity, indicating enhanced crystallinity.

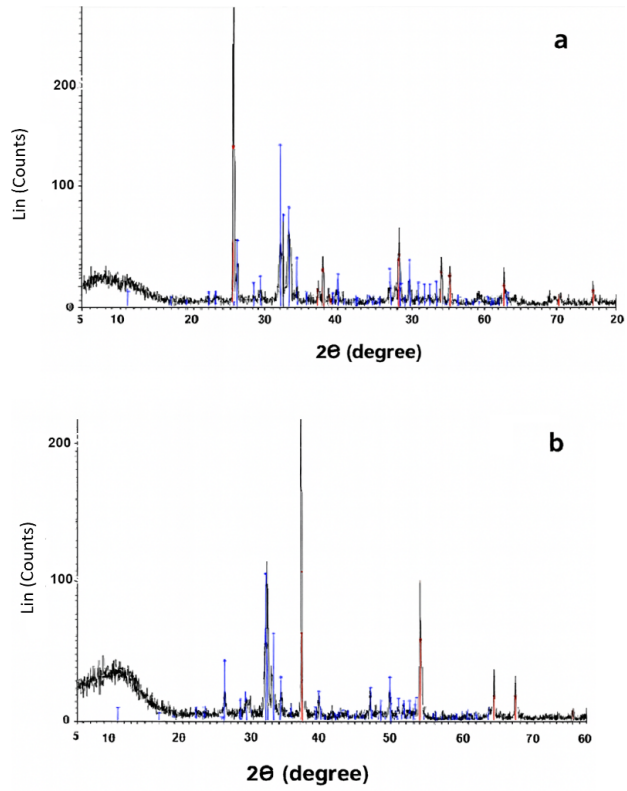

Figure 3. XRD patterns of the synthesized hydroxyapatite: (a) hydroxyapatite containing titanium oxide nanoparticles, (b) hydroxyapatite without titanium oxide nanoparticles.

3.4 Thermal analysis

Figure 4 presents the thermogravimetric analysis (TGA) curves of the hydroxyapatite samples synthesized with and without titanium oxide over the temperature range of 0-800 °C. Based on the figure, it can be observed that the hydroxyapatite synthesized in the presence of titanium oxide exhibits higher thermal stability compared to the sample synthesized without titanium oxide. As shown in the diagram, the weight loss with increasing temperature is greater in the hydroxyapatite sample without titanium oxide.
However, both samples demonstrate acceptable thermal stability, which may be attributed to successful synthesis, appropriate mechanical properties of the hydroxyapatite powders, the presence of hydroxyl groups, and the overall homogeneous and robust structure of the synthesized ceramic powders. Since the samples were not pre-dried, an endothermic reaction is observed between 50 °C and 200 °C, most likely due to the evaporation of residual moisture in the gel. In the temperature range of 200–600 °C, both endothermic and exothermic reactions appear, which may be related to the decomposition of heavier organic components.

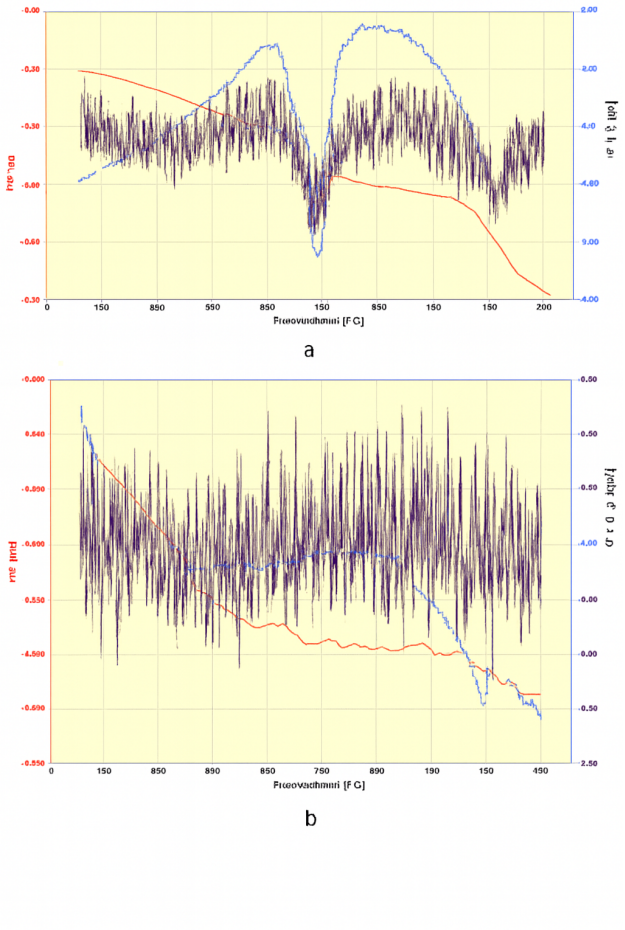

Figure 4. Thermogravimetric analysis (TGA) curves of the synthesized hydroxyapatite: (a) hydroxyapatite containing titanium oxide nanoparticles, (b) hydroxyapatite without titanium oxide nanoparticles.

3.5 Evaluation of cell viability

According to the results presented in figure 5, the survival and proliferation of osteoblasts cultured on both synthesized hydroxyapatite samples indicate that the powders produced—with and without titanium oxide-are biocompatible. Overall, the presence of a hydroxyapatite substrate significantly enhances cell growth and viability compared to the control wells without substrates. This positive effect of hydroxyapatite may be attributed to the release of calcium ions.

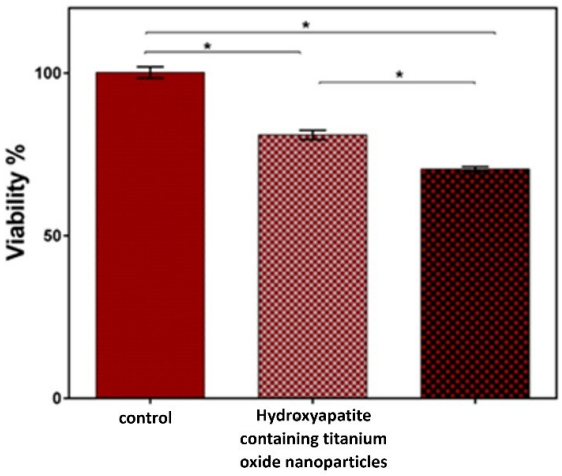

Figure 5. MTT assay results for evaluating the cell viability on the synthesized hydroxyapatite samples.

Consistent with the results of other experiments, the sample synthesized with added titanium oxide demonstrated superior biocompatibility. The cell viability on the hydroxyapatite substrate containing titanium oxide reached 82% $\pm$ 4.1, compared to 71% $\pm$ 3.8 for the sample synthesized without titanium oxide. Statistical analysis using the Student's t-test confirmed that this difference was significant ($p < 0.05$), indicating that TiO_2 incorporation enhances osteoblast viability.

3.6 Comparison with reported literature

To contextualize our results, Table 1 compares our TiO_2-modified hydroxyapatite with relevant reports on HAp powders, coatings, and composites used in dentistry. Relative to undoped HAp, our sol–gel TiO_2–HAp exhibits improved thermal stability and statistically higher osteoblast viability, supporting its suitability for dental restorations and implant coatings.

Table 1. Comparative literature table for dental hydroxyapatite systems.

Study	System/material	Synthesis route	Key findings	Relevance to dentistry
This work	HAp with TiO_2 nanoparticles (sol–gel)	Sol–gel incorporation of TiO_2 into HAp	Nanoparticles $\sim$ 57 nm; improved thermal stability with TiO_2; osteoblast viability 82% vs. 71% ($p < 0.05$)	Promising for restorations and coatings due to enhanced stability and biocompatibility
(Abidi and Murtaza, 2014)	Nano-HAp (no TiO_2)	Wet chemical precipitation	Controlled nano-HAp synthesis; phase-pure HAp; particle-size control reported	Baseline for HAp powders used in composites and pastes
(Awasthi et al., 2020)	HAp coatings (review)	Various coating methods	Summarizes adhesion, crystallinity, corrosion resistance; process–property relations	Guidance for optimizing HAp-coated implants and enamel-like layers
(Ma et al., 2017)	Modified HAp/PEEK biocomposites	Melt compounding/processing	Enhanced mechanical performance via HAp surface modification within PEEK	Load-bearing dental components and prosthetics with improved toughness
(Balhuc et al., 2021)	HAp nanoparticles in dental applications (review)	Various routes	Bioactivity, remineralization potential, antibacterial strategies	Direct use in toothpaste, varnishes, remineralization treatments
(Anil et al., 2022)	Nano-HAp for early caries remineralization	Formulation for topical use	Demonstrated enamel remineralization efficacy of nano-HAp	Non-invasive caries management; chairside applications
(Homa et al., 2024)	nHAp-functionalized titanium implants	Surface functionalization	Improved osseointegration; bioactive interface formation	Endosseous dental implants with enhanced bone contact
(Seesala et al., 2023)	Gradient HAp coating on zirconia implants	Coating/gradients	Stress distribution optimization; durable interface	Zirconia implants with tailored HAp layers for longevity
(Gaihre and Jayasuriya, 2018)	HAp-based composite scaffolds	Scaffold fabrication	Osteoconductivity; controlled porosity; mechanical tuning	Regenerative dentistry: bone defect repair scaffolds

Notes: Where specific numeric values (e.g., particle size distributions, viability percentages) are not reported in the cited works, findings are summarized qualitatively to avoid overinterpretation.

4. Conclusion

This study successfully synthesized a nano-hydroxyapatite composite doped with titanium oxide nanoparticles using the sol–gel method. Structural characterization confirmed the formation of a stable hydroxyapatite phase with enhanced crystallinity and strong interfacial bonding between TiO_2 and the HAp matrix. Thermal analysis revealed that TiO_2 incorporation significantly improved the thermal stability of the composite, while SEM imaging demonstrated uniform nanoparticle distribution and nanoscale morphology. Importantly, cytotoxicity testing using osteoblast cells showed excellent biocompatibility, with cell viability reaching 82% for the TiO_2-doped sample. These results collectively indicate that the synthesized composite exhibits superior physicochemical and biological properties compared to undoped hydroxyapatite. Therefore, TiO_2-modified hydroxyapatite presents a promising candidate for advanced dental restoration, implant coatings, and regenerative biomedical applications. Future studies may focus on in vivo performance, mechanical testing under load-bearing conditions, and long-term biological interactions to further validate its clinical potential.

Acknowledgements
The authors would like to thank Islamic Azad University, Yazd Branch, for their financial support throughout this research.

Authors contributions
Authors have contributed equally in preparing and writing the manuscript.

Availability of data and materials
The data that support the findings of this study are available from the corresponding author, upon reasonable request.

Conflict of interests
The authors declare that they have no known competing financial interests or personal relationships that could have appeared to influence the work reported in this paper.

References

Abdal-hay A., Hamdy A. S., Abdellah M. Y., Lim J. (2014) *In vitro* bioactivity of implantable Ti materials coated with PVAc membrane layer. *Mater Lett* 126:267–270. DOI: https://doi.org/10.1016/j.matlet.2014.04.097.

Abidi S. S., Murtaza Q. (2014) Synthesis and characterization of nano-hydroxyapatite powder using wet chemical precipitation reaction. *J Mater Sci Technol* 30:307–310. DOI: https://doi.org/10.1016/j.jmst.2013.11.005.

Albulescu R., Popa A. C., Enciu A. M., Albulescu L., Dudau M., Popescu I. D., et al. (2019) Comprehensive in vitro testing of calcium phosphate-based bioceramics. *Materials* 12:3704. DOI: https://doi.org/10.3390/ma12223704.

Alzahrani T. M., Jumah A. A., Alshehri F. A., Alshiha S. A. (2022) Assessment of the economic burden of dental diseases. *Saudi J Oral Dent Res* 7:220–224. DOI: https://doi.org/10.36348/sjodr.2022.v07i09.002.

Anil A., Ibraheem W. I., Meshni A. A., Preethanath R. S., Anil S. (2022) Nano-hydroxyapatite in early dental caries remineralization. *Int J Environ Res Public Health* 19 (9): 5629. DOI: https://doi.org/10.3390/ijerph19095629.

Awasthi S., Pandey S. K., Arunan E., Srivastava C. (2020) A review on hydroxyapatite coatings. *J Mater Chem B,* DOI: https://doi.org/10.1039/D0TB02407D.

Balhuc S., Campian R., Labunet A., Negucioiu M., Buduru S., Kui A. (2021) Dental applications of hydroxyapatite nanoparticles. *Crystals* 11 (6): 674. DOI: https://doi.org/10.3390/cryst11060674.

Beig B., Liaqat U., Khan Niazi M. F., Douna I., Zahoor M., Khan Niazi M. B. (2020) Challenges and developments in hydroxyapatite coatings. *Coatings* 10:1249. DOI: https://doi.org/10.3390/coatings10121249.

Blatz M. B., Chiche G., Bahat O., Roblee R., Coachman C., Heymann H. O. (2019) Evolution of aesthetic dentistry. *J Dent Res* 98:1294–1304. DOI: https://doi.org/10.1177/0022034519875450.

Chamrad J., Marcian P., Cizek J. (2021) Hydroxyapatite coating for cranial implant. *PLoS ONE* 16:e0254837. DOI: https://doi.org/10.1371/journal.pone.0254837.

Chen L., Zhai D., Huan Z., Ma N., Zhu H., Wu C., et al. (2015) Silicate bioceramic/PMMA bone cement. *RSC Adv* 5:37314–37322. DOI: https://doi.org/10.1039/C5RA04083J.

Demarco F. F., Conde M. C. M., Cavalcanti B. N., Casagrande L., Sakai V. T., Nör J. E. (2011) Dental pulp tissue engineering. *Braz Dent J* 22:3–13. DOI: https://doi.org/10.1590/S0103-64402011000100001.

Eliaz N., Metoki N. (2017) Calcium phosphate bioceramics review. *Materials* 10:334. DOI: https://doi.org/10.3390/ma10030334.

Filip D. G., Surdu V. A., Paduraru A. V., Andronescu E. (2022) Hydroxyapatite and bioglass developments. *J Funct Biomater* 13 (4): 248. DOI: https://doi.org/10.3390/jfb13040248.

Gaihre B., Jayasuriya A. C. (2018) Composite scaffolds for bone regeneration. *Mater Sci Eng C* 91:330–339. DOI: https://doi.org/10.1016/j.msec.2018.05.060.

Guma T. N., Madakson P. B., Yawas D. S., Aku S. Y. (2012) X-ray diffraction analysis of the microscopies of some corrosion-protective bitumen coatings. *Int J Mod Eng Res* 2 (6): 4387–4395.

Guo L., Li B., Zhang C. (2020) Hydroxyapatite via sol–gel method: optimization. *J Sol-Gel Sci Technol,* DOI: https://doi.org/10.1007/s10971-020-05381-1.

Hanawa T. (2020) Zirconia vs. titanium in dentistry. *Dent Mater J* 39 (1): 24–36. DOI: https://doi.org/10.4012/dmj.2019-172.

Homa K., Zakrzewski W., Dobrzyński W., Piszko P. J., Piszko A., Matys J., Wiglusz R. J., Dobrzyński M. (2024) Nanohydroxyapatite-functionalized titanium implants. *J Funct Biomater* 15:45. DOI: https://doi.org/10.3390/jfb15020045.

Hung M., Lipsky M. S., Moffat R., Lauren E., Hon E. S., Park J., et al. (2020) Health and dental care expenditures. *PLoS ONE* 15:e0234459. DOI: https://doi.org/10.1371/journal.pone.0234459.

Hussein A. I., Che Mat A. N., Abd Wahab N. A. A., Ab-Rahman I., Husein A., Ab-Ghani Z. (2020) Calcia-stabilized zirconia for dental applications. *Appl Sci* 10:5751. DOI: https://doi.org/10.3390/app10175751.

Iftikhar S., Jahanzeb N., Saleem M., ur Rehman S., Matinlinna J. P., Khan A. S. (2021) Trends in dental biomaterials research. *Saudi Dent J* 33 (4): 229–238. DOI: https://doi.org/10.1016/j.sdentj.2021.01.002.

Ignjatović N., Tomić S., Dakić M., Miljković M., Plavšić M., Uskoković D. (1999) Hydroxyapatite/PLLA composite biomaterials. *Biomaterials* 20:809–816. DOI: https://doi.org/10.1016/S0142-9612(98)00234-8F.

Janakiram C., Antony B., Joseph J., Ramanarayanan V. (2018) Dental caries prevalence in India. *J Clin Diagn Res* 12 (8): ZE08–ZE13. DOI: https://doi.org/10.7860/JCDR/2018/32669.11956.

Jarcho M., Bolen C. H., Doremus R. H. (1976) Hydroxyapatite synthesis. *J Mater Sci* 11

Jevdjevic M., Listl S., Beeson M., Rovers M., Matsuyama Y. (2020) Forecasting dental health expenditures. *Community Dent Oral Epidemiol,* DOI: https://doi.org/10.1111/cdoe.12597.

Kaneko T., Gu B., Sone P. P., Zaw S. Y. M., Murano H., Zaw Z. C. T., Okiji T. (2018) Dental pulp tissue engineering using MSCs. *Stem Cell Rev Rep* 14:668–676. DOI: https://doi.org/10.1007/s12015-018-9828-6.

Lewallen E. A., Jones D. L., Dudakovic A., Thaler R., Paradise C. R., Kremers H. M., et al. (2016) MSCs on 3D-printed titanium. *Gene* 581:95–106. DOI: https://doi.org/10.1016/j.gene.2016.01.015.

Ma R., Li Q., Wang L., Zhang X., Fang L., Luo Z., Xue B., Ma L. (2017) Modified-HA/PEEK biocomposites. *Mater Sci Eng C* 73:429–439. DOI: https://doi.org/10.1016/j.msec.2016.12.076.

Murad A. H., Fadhala H. F. (2023) Immunomodulatory biomaterials in dental pulp regeneration. *Future Dent Res* 1 (1): 1–11. DOI: https://doi.org/10.57238/fdr.2023.144820.1000.

Praveen P., Viruthagiri G., Mugundan S., Shanmugam N. (2014) Structural, optical and morphological analyses of pristine titanium dioxide nanoparticles synthesized via sol–gel route. *Spectrochimica Acta Part A: Molecular and Biomolecular Spectroscopy* 117:622–629. DOI: https://doi.org/10.1016/j.saa.2013.09.037.

Pushpalatha C., Gayathri V. S., Sowmya S. V., Augustine D., Alamoudi A., Zidane B., et al. (2023) Nanohydroxyapatite in dentistry: review. *Saudi Dent J* 35:741–752. DOI: https://doi.org/10.1016/j.sdentj.2023.05.018.

Ramesh S., L. Aw. K., Tolouei R., Amiriyan M., Tan C. Y., Hamdi M., et al. (2013) Sintering properties of hydroxyapatite. *Ceram Int* 39:111–119. DOI: https://doi.org/10.1016/j.ceramint.2012.06.085.

Roberts W. E., Mangum J. E., Schneider P. M. (2022) Pathophysiology of demineralization. *Curr Osteoporos Rep* 20:106–119. DOI: https://doi.org/10.1007/s11914-022-00723-0.

Roveri N., Battistella E., Bianchi C. L., Foltran I., Foresti E., Iafisco M., et al. (2017) Surface enamel remineralization. *Materials* 10 (3): 334. DOI: https://doi.org/10.3390/ma10030334.

Seesala V. S., Rajasekaran R., Ojha A. K., Mahato A., Korrayi R. R., Das B., et al. (2023) Gradient hydroxyapatite coating for zirconia implants. *Surf Coat Technol* 469:129817. DOI: https://doi.org/10.1016/j.surfcoat.2023.129817.

Silva C. R., Gomez-Florit M., Babo P. S., Reis R. L., Gomes M. E. (2018) 3D scaffolds for dental engineering. In Functional 3D Scaffolds. 423–450. DOI: https://doi.org/10.1016/B978-0-08-100979-6.00018-1.

Soysal K., Park J., You S. H., Shin D. W., Bae W. T., Ozturk A. (2011) Preparation and photocatalytic activity of apatite precipitated TiO_2. *Journal of Ceramic Processing Research* 12:176–182.

Syed M. R., Bano N. Z., Ghafoor S., Khalid H., Zahid S., Siddiqui U., et al. (2020) Bioactive glass fiber composite. *Ceram Int* 46:21623–21631. DOI: https://doi.org/10.1016/j.ceramint.2020.05.268.

Weng W., Shen G., Han G. (2000) Low-temperature HA coatings on titanium. *Mater Lett* 19:2187–2190. DOI: https://doi.org/10.1016/S0167-577X(00)00362-0.

Wolf T. G., Cagetti M. G., Fisher J.-M., Seeberger G. K., Campus G. (2021) Oral health & NCDs overview. *Front Oral Health* 2:725460. DOI: https://doi.org/10.3389/froh.2021.725460.